Title

Electroreduction of Captured CO2 on Silver Catalysts: Influence of the Capture Agent and Proton Source

Journal

Journal of the American Chemical Society, 146(30)

ISSN

0002-7863

Authors

Kowalski, Robert Michael
Banerjee, Avishek
Yue, Chudi
et al.

Publication Date

2024-07-31

DOI

10.1021/jacs.4c03915

Electroreduction of Captured CO_2 on Silver Catalysts: Influence of Capture Agent and Proton Source.

Robert Michael Kowalski,[a, †] Avishek Banerjee,[a, †] Chudi Yue,[a] Sara G. Gracia,[a] Dongfang Cheng,[a] Carlos G. Morales-Guio, [a,*] and Philippe Sautet[a,b,c,*]

[a] Department of Chemical and Biomolecular Engineering, University of California, Los Angeles, CA 90095, United States
[b] Chemistry and Biochemistry Department, University of California, Los Angeles, CA 90095, United States
[c] California NanoSystems Institute, University of California, Los Angeles, CA 90095, United States
*Corresponding authors: Philippe Sautet (sautet@ucla.edu), Carlos G. Morales-Guio (moralesguio@ucla.edu)
[†] These authors contributed equally to this work

Abstract

In the context of carbon reutilization, the direct electroreduction of captured CO_2 (c-CO_2RR) appears as an appealing approach since it avoids the energetically costly separation of CO_2 from the capture agent. In this process, the CO_2 is directly reduced from its captured form. Here we investigate the influence of the capture agent and proton source on that reaction from a combination of theory and experiment. Specifically, we consider methoxide captured CO_2, NH_3 captured CO_2, and bicarbonate on silver electrocatalysts. We show that the proton source plays a key role in the interplay of the chemistries for the electroreduction of protons, of free CO_2, and of captured CO_2. Our density functional theory calculations, including the influence of the potential, demonstrate that a proton source with smaller pK_a improves the reactivity for c-CO_2RR , but also increases the selectivity towards HER on silver surfaces. Since c-CO_2RR requires an additional chemical protonation step, the influence of the proton source is stronger than for HER. However, c-CO_2RR cannot compete with HER on Ag, Experimentally, the dominant product observed is H_2 with low amounts of CO being produced. Through a rotating cylinder electrode cell of well-defined mass transport properties, we conclude that although methanol solvent exhibits a lower HER activity, HER remains dominant over c-CO_2RR. Our work suggests that methoxide is a potential alternative capture agent to NH_3 for direct reduction of captured CO_2, though challenges in catalyst design—particularly in reducing the onset potential of c-CO_2RR to surpass HER—remain to be addressed.

Introduction

Over the past 100 years the concentration of atmospheric CO_2 has risen as the world has undergone widespread industrialization.[1] Fossil fuels are currently the leading source of energy, but the major byproduct of burning these fuels is CO_2. This has led to changes in the climate and

thus, efforts to decrease the CO_2 concentration in the atmosphere have undergone intense study. Currently, the main pathway to utilize the net flux of anthropogenic carbon getting in the atmosphere is carbon capture and utilization (CCU). In CCU, the CO_2 is captured and used for fuel or chemical production.[2] Significant work has been done on directly reducing CO_2 (CO_2 reduction reaction, CO_2RR) via thermocatalytic or electrocatalytic routes to upgrade CO_2 to CO, C_1, and C_{2+} products.[3–7] For the most part, catalytic routes have been developed to start from a pure and concentrated source of CO_2. In CCU processes, CO_2 must first be captured from a diluted exhaust stream, for example by forming a complex with a capture agent, and then CO_2 must be released to produce high concentration CO_2 for the reduction reaction.[8] Releasing the captured CO_2 is an endergonic process requiring a large amount of energy.[9] It might therefore be energetically advantageous to directly transform captured CO_2, in the complex with the capture agent, a process we label here as the direct reduction reaction of captured CO_2 (c-CO_2RR).

Commonly, amines have been used to capture CO_2 and produce carbamate adducts.[10] These have proven to be effective capture agents as they bind strongly to CO_2 through the formation of a covalent C-N bond.[11,12] However, when it becomes desirable to directly reduce the captured CO_2 complex, this stability of the C-N bond becomes an extra challenge, imposing a larger overpotential for an electrocatalyst to drive the transformation of the bound CO_2 molecule.[13] Another problem that arises from the capture chemistry itself is that it requires 2 equivalents of amine to capture 1 equivalent of CO_2.[12] In the carbamate formation reaction, one ammonium cation is produced as a byproduct for each CO_2 molecule captured.[12,14] It could be possible to use this cation as a proton source for the reduction of carbamate adducts, but the effect that the proton source has on c-CO_2RR has not been explored. Multiple proton donor species are indeed generated in aqueous amine-based CO_2 capture solutions including bicarbonates, ammonium cations and hydronium ions and their population will be the result of competing buffering reactions facilitated by the water dissociation reaction.[15] In amine-based c-CO_2RR systems, what is more commonly seen is the competing hydrogen evolution reaction (HER)[15,16] and most of the CO produced comes from the electrochemical reduction of the dissolved "free" CO_2 in equilibrium with the carbamate.[17] At a rough approximation, two of the major handles for the design of c-CO_2RR systems could be i) the strength and nature of the bond (covalent vs. ionic) between the C atom in CO_2 and a heteroatom in the capture agent (e.g. O, C, N, P, S), and ii) the proton source used during the electrochemical reduction of the CO_2 adduct. To start to understand the various c-CO_2RR design parameters, it is necessary to consider other families of capture agents beyond amines and hydroxyls.

Alcohols offer an alternative as capture agent. Unlike amines, only one alcohol is required to capture one CO_2 to produce one carbonate molecule.[12] Although, the binding energy between alcohols and CO_2 is typically smaller than that between amines and CO_2,[12] this may prove energetically beneficial when trying to directly reduce the carbonate complex without separation of CO_2. A smaller binding energy could result in slower kinetics for CO_2 capture, but these could be offset by the higher solubility of CO_2 in less polar solvents compared to water.[18] While alcohols could pose additional challenges related to anode chemistries and systems complexity including solubility of CO_2 capture species, their exploration remains highly valuable. This is because alcohols can access pKa regions potentially conducive to suppressing the HER and enhancing the

viability of c-CO_2RR pathways. The study of c-CO_2RR in alcohols offers an additional space to understand the effect of the proton source on the overall c-CO_2RR reaction network. As the pK_a of a proton source is decreased, the ability of that proton source to donate its proton should increase. However, the HER, CO_2RR and c-CO_2RR all require multiple protonation steps per catalytic cycle.[17,19,20] Thus, it is important to determine how the proton source will affect the reactivity of these different capture agents and to further explain what challenges remain in optimizing reaction conditions for c-CO_2RR in competition with HER.

In this work, grand canonical density functional theory (GCDFT) and experiments are combined to compare the direct electroreduction of methoxide captured CO_2, NH_3 captured CO_2, and bicarbonate. Methyl carbonate and potassium carbamate were chosen as they are the simplest representative of CO_2 captured complexes with alcohol and amine families. The catalyst selected for this comparison is Ag as this metal has a high overpotential for the competing HER.[21,22] The main objective of our research is to determine if the overpotentials for direct reduction of captured CO_2 can be brought low enough to compete with the HER. Experimentally, we observe that although HER can be suppressed in the presence of methanol as the solvent, HER is generally more facile than c-CO_2RR for all the capture agents investigated here. In all cases, detailed measurements of the dissolved CO_2 in equilibrium with the solution reveal that the active species to produce CO is the dissolved CO_2 while the c-CO_2RR pathways remained kinetically prohibited. Thus, the goal of this work is threefold: i) to systematically explore the potential for the reactive capture of CO_2 with alcohol-based capture agents, in comparison with amines and water, ii) to elucidate the effect of the proton source on the overall reaction network for the electroreduction of captured CO_2, iii) to understand the mechanism for c-CO_2RR on Ag catalysts by using DFT in order to provide insights and trends of proton-source and capture agent influence and underline limiting factors for c-CO_2RR.

Methods

Experimental

Preparation of Catalysts

Silver (Ag) electrocatalysts used in the experiments were prepared by sputtering Ag onto Titanium (Ti) cylinder electrodes. The cylinder substrates have an outer diameter of 12 mm and outer active surface area of 3 cm^2. The Denton Vacuum Discovery 550 Sputtering system was used for the sputtering of the Ag metal. This system is equipped with two direct current (DC) guns and two radio frequency (RF) guns which bombard Ag targets onto the Ti substrates. The RF gun was used to sputter a 100 nm Ti adhesion layer and the DC gun was used to sputter the Ag target on our electrodes. An initial Ar sputtering was performed to remove native oxide layers on the titanium cylinders. The Ar sputtering was followed by the deposition of a 100 nm layer of sputtered Ti on the substrate to enhance adhesion of the Ag metal. 500 nm of Ag was then sputtered onto the electrodes to make the Ag catalyst as shown in the digital image in Figure S1a. The as-sputtered electrodes are not atomically flat, and their roughness factor is 2.56 as determined by measuring

the double layer capacitance of the Ag electrodes (Figure S1c). The double layer capacitance of an atomically flat Ag electrode is assumed to be 30 μF/cm^2.[31]

In order to investigate the effect of the catalyst porosity for c-CO_2RR, we have also prepared a silver catalyst electrode of a higher roughness factor. A 0.2 M KOH was used as an electrolyte with a Pt counter and a Ag/AgCl reference electrode to perform a surface roughening process on the sputtered Ag film (Figure S1b). Here, the sputtered Ag cylinder was used as the working electrode. The surface roughening was conducted using consecutive oxidative and reductive cycles as shown in Figure S1b. 15 cycles of cyclic voltammetry were conducted to roughen the surface of the Ag cylinder. The roughness factor of the nanoporous Ag was measured to be 29.8 from the double layer capacitance (Figure S1c) compared to an atomically flat Ag electrode (30 μF/cm^2).

Electrochemical Characterization

A three-electrode gas-tight rotating cell setup was used with the Ag cylinder as the working electrode, a platinum foil (Pt, 0.1 mm thick, 99.99% metal basis, Alfa Aesar) as the counter electrode, and the Ag/AgCl/1 M KCl as the reference electrode (CH Instruments, Inc.) as shown in Figure S3. Potassium Bicarbonate ($KHCO_3 \geq 99.95\%$, Sigma-Aldrich), Ammonium Carbamate (NH_4-NH_2CO_2) (≥ 98%, Thermo-Fischer), and 25 wt% potassium methoxide (CH_3OK) in Methanol (≥ 99.9%, Sigma-Aldrich) were chosen as the electrolytes for c-CO_2RR studies. 0.5 M $KHCO_3$ was prepared in water. The 0.5 M NH_4-NH_2CO_2 electrolyte was prepared by dissolving the ammonium carbamate salt in water along with potassium perchlorate $KClO_4$ (99.99%, Thermo-Fischer) as the supporting electrolyte. Potassium hydroxide KOH (99.97%, Sigma-Aldrich) was added before the addition of the ammonium carbamate to control the pH to an alkaline level before the dissolution of the carbamate. The nominal concentration of the ammonium carbamate, the perchlorate, and the potassium hydroxide is 0.5 M, 0.1 M and 0.001 M respectively. The ammonium carbamate electrolyte was freshly prepared before starting the experiments. 5 wt% CH_3OK was prepared in pure methanol solvent. For 5 wt% methoxide, CO_2 loading was performed using 70 sccm of CO_2 flow into the solution and the mass change was tracked until saturation (Figure S2). Infrared Spectroscopy was performed on the CO_2 loaded sample to verify the formation of methyl carbonate in the solution (Figure S4). All the solutions were purged with Argon (Ar, Airgas 99.999%) at 50 sccm for 15 mins to remove as much dissolved CO_2 as possible before doing electrochemistry, although the concentration of the dissolved CO_2 does equilibrate quickly with the captured CO_2-adduct within a few minutes. The solution was then transferred to the RCE cell and constant potential chronoamperometry was performed under constant Ar flow. The potential was fixed at -1.3 V, -1.5 V, -1.8 V, and -2 V vs Ag/AgCl for the bicarbonate and ammonium carbamate capture agent, and it was fixed at -1.5 V, -1.8 V, -2 V, and -2.2 V vs Ag/AgCl for methyl carbonate capture agent. Electrochemical impedance spectroscopy (EIS) was collected under each potential and the uncompensated resistance was determined from the real part of the resistance measured at high frequency ($f \geq$ 100kHz), which was then corrected from all chronoamperometry measurements. Four GC injections were collected in each experiment and the average of the last three data points were plotted in all the figures. A constant Ar flow of 20 sccm was maintained throughout all experiments with an electrode rotation speed of 800 rpm. The partial pressure of CO_2 in the headspace of the

cell was also measured with each GC injection to determine the amount of dissolved CO_2 in equilibrium with the captured CO_2 in the bulk of the electrolyte.

Product Characterization

A gas chromatograph (model 8610C, SRI Instruments) was used to identify and measure the gas products. The injections were administered at 20-minute intervals which included a 14-minute run phase of product separation in the chromatography column followed by a 6-minute cooling period. The signals from the thermal conductivity detector (TCD) and the flame ionization detector (FID) were collected and compared with the calibration curves to determine the Faradaic efficiency (FE) for various products like hydrogen (H_2) and carbon monoxide (CO). The minimum quantification limit for CO and H_2 is approximately 1 ppm and 100 ppm, corresponding to minimum quantifiable partial current densities of roughly 0.001 mA/cm² and 0.1 mA/cm², respectively, when normalized to our catalyst surface area. All the experimentally collected data is summarized in Table S1.

Transport-based Model Development to determine c-CO_2RR Activity

The gas-tight rotating cylinder electrode cell (RCE) was used for the experiments which has well defined mass-transport properties along with the ability to quantify both gas and liquid products during electrolysis. The relation between hydrodynamics (electrode rotation rate) and the mass transport film coefficient for charged and uncharged reactants in the RCE cell were described by Jang. *et. al.*. A dimensionless relation between Sherwood (Sh), Schmidt (Sc), and Reynolds (Re) numbers for the RCE cell was used to develop our own model to evaluate c-CO_2RR activity.[32] To define the activity for c-CO_2RR, it is important to understand the source of carbon in our experiments. In all systems investigated, whenever a CO_2 captured molecule like carbamate or carbonate is dissolved in a solution there exists an equilibrium which facilitates the existence of both the CO_2-bound adduct and unbound dissolved CO_2 in the solution. To determine the molecule getting reduced we carefully investigated and characterized the processes that take place at the gas-liquid interface and the liquid-electrode interface. In the gas-liquid interface, the concentration of unbound dissolved CO_2 is always in a pseudo-equilibrium with the partial pressure of CO_2 in the headspace which follows Henry's law, where H_{CO2}=0.034 M atm^{-1} for CO_2 in water, and H_{CO2}=0.18 M atm^{-1} for CO_2 in methanol at 293.15 K.[33,34]

The experimental challenge in c-CO_2RR systems is to measure the partial pressure of CO_2 in equilibrium with the unbound dissolved CO_2, which in this work was measured using a GC directly connected to the headspace of the cell. Thus, the concentration of unbound dissolved CO_2 in the solution can be calculated from the measured partial pressure of CO_2 in the headspace. Similarly, in the liquid-electrode interface, one can calculate the maximum flux of dissolved CO_2 supplied to the surface of the electrode once the amount of dissolved CO_2 in the bulk is known. The universal Sherwood number relationship developed by Jang. *et. al.* holds true regardless of the experimental conditions including the effects of reactants, their concentration, electrode rotation, and temperature, which was used as a reference to calculate the convective mass-transport

limited rates for CO_2 transport by eq 1 and 2. The CO_2 present at the surface of the electrode was considered to be 0 to obtain the maximum flux of CO_2. A transport-based line for the maximum partial current density for CO from the maximum flux of CO_2 can then be defined for different partial pressures of CO_2 at different rotation speeds as shown in Figure S5. It should also be noted that the diffusion coefficient of CO_2 in water is different from that of CO_2 in methanol ($D_{CO_2(water)}$=1.67×10^9 m^2 s^{-1} and $D_{CO_2(methanol)}$=4.75×10^9 m^2 s^{-1}).[35] In order to conclude that a catalyst is capable of driving the direct reduction of the CO_2-bound adduct, it would be necessary for the j_{CO} values measured in the RCE cell to be higher than the $j_{CO,max}$ value expected from the transport-based model.[17]

$$Sh_{RCE} = \frac{\frac{k_m}{D}}{d_{cyl}} = 0.204\, Re_{RCE}^{0.59}\, Sc^{0.33} \quad (1)$$

$$j_{CO,max} = nF C_{CO_2}^{bulk} k_{m,CO_2} \quad (2)$$

Computational

All computational work was carried out using density functional theory with the Perdew-Burke-Ernzerhof (PBE)[23] exchange correlation functional, in the framework of the Vienna *ab-initio* Simulation Package (VASP).[23,24] Van der Waals interactions were included using the D3 method.[25] It is important to underline that current exchange-correlation functionals include approximations so that error bars on absolute energies are ~0.2 eV. However, our conclusions only rely on energy differences between similar systems that could be more accurate, and in any case such errors on the energy do not affect qualitative results and comparisons in the paper.

The solvent was modelled as a dielectric continuum, and the electrolyte distribution was described with the linearized Poisson-Boltzmann equation, with the Debye screening length as main parameter.[26,27]

All Ag slabs in this work used a lattice constant of 4.09 Å. The influence of the potential was included by Grand-Canonical DFT where the number of electrons is modified to match the target potential. All slab models were symmetrical, i.e. presented equivalent surfaces on their top and bottom parts, to eliminate effects from a net dipole moment.[28–30] The super cell was 3x3 for the (111) surface and 2x3 for the (211) surface. The electronic energy was considered converged once the energy difference between consecutive electronic steps was less than 10^{-6} eV. All optimizations were considered converged when the maximum force was less than 0.02 eV/Å. For simplicity some calculations were first optimized on non-symmetric slabs, and then single point energy calculations were performed on symmetrized versions to include the influence of the potential by surface charging (Figure S15 for validation). The influence of the coverage of K was tested to be small on potassium methyl carbonate adsorption on Ag(111) (Figure S16) and it was decided to use a coverage of 1/9 ML. A detailed explanation of all computational parameters, images of all structures used, as well as the optimized structure files can be found in the supplementary information.

Results and Discussion

Reaction Mechanism

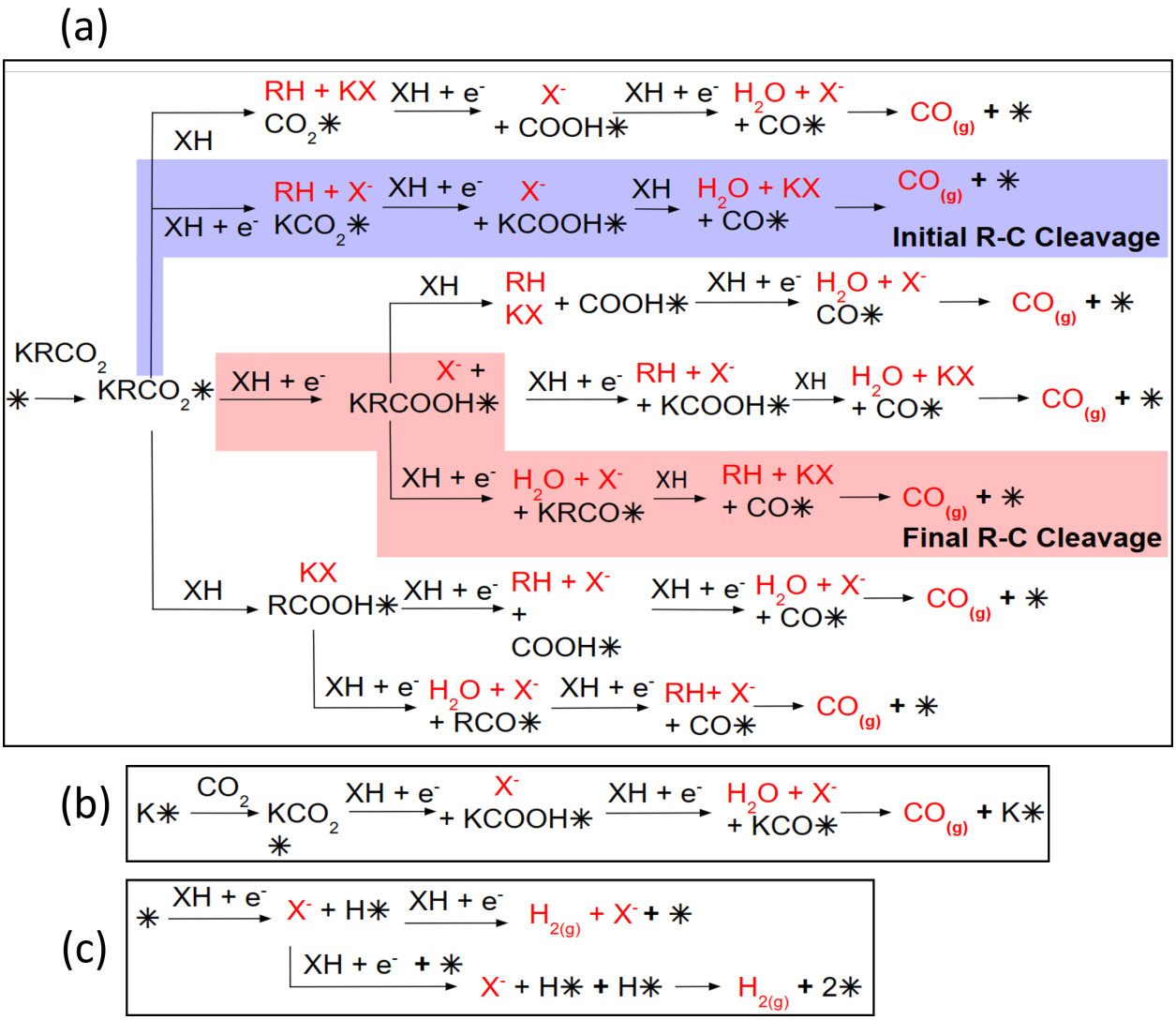

Figure 1: (a) Reaction scheme for the reduction of the captured CO_2 with a general capture agent (R-H, examples being NH_2-H, CH_3O-H, HO-H). R represents the deprotonated capture agent (NH_2 for NH_3, OCH_3 for methanol or OH for H_2O), XH represents a general proton source. In methanol solvent the proton sources in our study include methanol and NH_4^+, written formally NH_4ClO_4 to be in the XH form. In the water-amine solvent this includes H_2O, $KHCO_3$, and NH_4^+. * represents the catalytic Ag site. All species containing * are absorbed on the site. Chemicals in red text represent the products evolving in the solvent at each step. The two most favored pathways from our calculations both initiate with a proton coupled electron transfer and are highlighted in blue (initial R-C cleavage in the CO_2 complex) or in red (final R-C cleavage). Reaction schemes for (b) CO_2RR, and (c) HER are also recalled with similar notations.

When CO_2 is complexed by a generic capture agent (noted here R-H), a R-CO_2^- adduct anion is formed. If coupled with a potassium cation in an ion pair $KRCO_2$, the general half-cell reaction for the direct electroreduction of the adduct in basic conditions with the proton source XH formally reads:

$$KRCO_2 + 3XH + 2e^- \rightarrow CO + H_2O + RH + KX + 2X^- \qquad (3)$$

The capture agent RH is reformed, CO is produced, and the reaction involves two electrons. For the ammonia capture agent, used as a model amine, R = NH_2, while for methanol, used as a model alcohol, R = OCH_3. Depending on the solvent and capture agent, the proton source XH can be methanol, NH_4ClO_4, H_2O or $KHCO_3$. For the systems in this work the captured CO_2 complex $KRCO_2$ refers to either potassium methyl carbonate (R= CH_3O), potassium bicarbonate (R=HO), or potassium carbamate (R=NH_2). Potassium is chosen as the alkali cation because it is part of the $KClO_4$ supporting electrolyte and because of previous work detailing its potential effectiveness on similar systems compared to other alkali metals such as sodium and lithium.[17,36–39] K in this work is considered to be always in its cationic K^+ state as the equilibrium potential for the reduction of K^+ is more negative than the considered potentials. $KRCO_2$ for example indicates $K^+RCO_2^-$ in a usual simplified notation.

Elementary reaction steps include two electrochemical proton coupled electron transfers (PCET) and one chemical protonation. Figure 1a depicts various possibilities to combine these elementary steps in a generic reaction network. After adsorption of the CO_2 complex $KRCO_2$ on the Ag electrode, forming $KRCO_2$*, four possible reaction paths can occur. The top route starts with a cleavage of the R-C bond assisted by protonation using the proton source XH, yielding adsorbed CO_2, RH and KX. From there the usual CO_2RR pathway follows, with a first PCET yielding *COOH, and a second producing water and *CO which desorbs to restore the bare site. The second pathway is similar in the bond breaking and forming sequence but modifies the order of PCET and protonation, starting by a PCET assisted cleavage of the R-C bond, followed by a second PCET to form *COOH, while the final step of C-O bond cleavage is chemically assisted by a proton transfer from XH. An alternative would be to place the chemical protonation step in the middle, but this is omitted here for simplicity. The third route differs since it starts with a PCET at an O atom forming KRCOOH. From there three routes are possible: A PCET can cleave the C-OH bond to form RCO, and the R-C bond is broken in a final chemical proton transfer step producing CO, water and KX. Alternatively, the R-C bond can be broken first, either by PCET or proton transfer, followed by the C-O bond cleavage, also either by PCET or proton transfer (whatever remains available). The fourth pathway is similar to the third one but treats the first step as a chemical protonation at O using the XH proton source. In return the second and third steps can be electrochemical PCET.

Competitive pathways are the CO_2RR from dissolved CO_2 in equilibrium with the complex with the capture agent and the HER, shown in Figures 1b and 1c, respectively. HER and CO_2RR also require two PCET per cycle, since CO_2RR on Ag stops at the CO product. For the HER, a PCET first electrochemically absorbs a proton onto the surface. This is followed by a second PCET which can either immediately produce H_2 (Volmer-Heyrovsky mechanism) or add an additional H adsorbed to the surface. These two H atoms then combine to produce gaseous H_2

(Volmer-Tafel mechanism). Ag was chosen as the catalyst because of its significant overpotential for HER, since the H binding to Ag is much weaker than that of Pt, which is a well-known metal for optimum H binding.[21,22] Thus, it is desirable to determine if this overpotential for HER is large enough to allow for the reduction of captured CO_2 to occur. For the CO_2RR, first the CO_2 is absorbed to the surface where it then undergoes two PCET steps to be reduced into CO. The K^+ cation improves the activity of CO_2RR, from experiments[38] and from our calculations, and thus is taken to always be present in our calculations for the CO_2RR.

The proton source significantly impacts the reaction steps. The chemical potential of a coupled proton and electron is determined by the equilibrium with H_2 gas at the hydrogen electrode as shown in equation 4 (with the potential U expressed versus SHE)[40]

$$\Omega_{H^+/e^-} = \frac{1}{2}\Omega_{H_2} - eU - \ln(10)\, k_B T pH \quad (4)$$

Even when other proton sources XH are used, equation 4 holds valid for the chemical potential of the coupled proton and electron. This is because the proton and the X^- anion can be reformed to make the XH proton source. Thus, for all calculations, PCET steps will be modeled by equation 4.

However, as shown in Figure S6 the onset potential of the HER can be shifted by the pK_a of the proton source. The addition of a negatively charged buffer or a neutral molecule does not change the onset potential for HER and this onset primarily depends on the pKa of the proton source (Figure S7). Thus, in equation 4 the pH term can be substituted with the desired proton source's pK_a. Thus, what will occur is that as the proton source's pK_a is decreased the chemical potential of the coupled proton and electron will decrease. As the protons are always reactants, a decrease in proton source pK_a will improve the overall reaction energy. In this work, there were four proton sources considered (methanol, H_2O, $KHCO_3$, and NH_4ClO_4), each with a different pK_a.

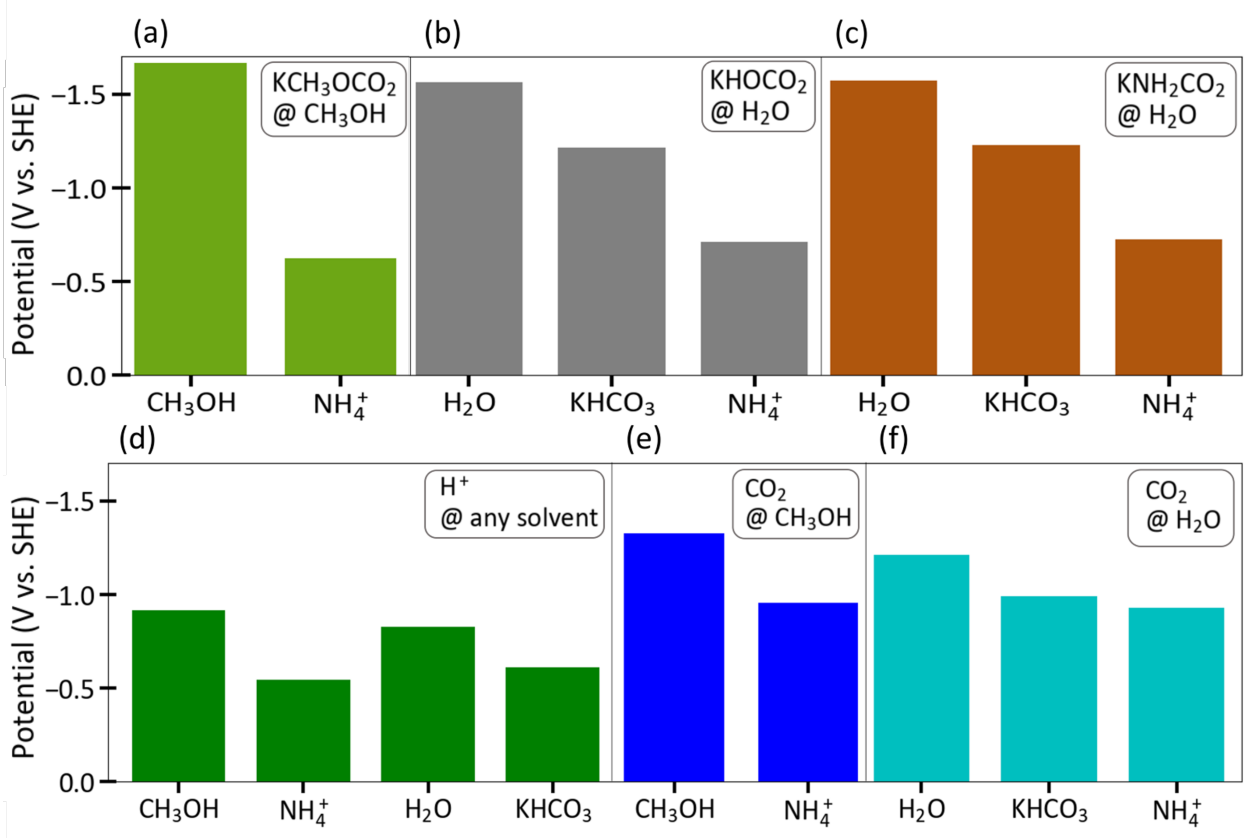

Figure 2: Calculated equilibrium potential for the electroreduction to CO of (a) methyl carbonate KCH_3OCO_2 (b) bicarbonate $KHOCO_2$, (c) carbamate KNH_2CO_2, compared to that for (d) HER, (e and f) CO_2RR to CO. The compound being electrochemically reduced is labeled in the top right of each panel, together with the solvent (notation: compound@solvent). The x axis denotes the proton source for the electrochemical reduction. The overall reaction energy as a function of potential is given in Figure S17. KCH_3OCO_2 indicates $K^+CH_3OCO_2^-$ etc.

To start our analysis, the first step is to consider the overall thermodynamics of the catalytic reactions, that is, to determine the equilibrium potential of c-CO_2RR with our different capture agents, as shown with different colors in Figure 2. The calculated thermodynamics for c-CO_2RR strongly depends on the nature of the proton source, the ammonium cation being most favorable i.e. providing the least negative equilibrium potential (Figure 2 a-c). The product of the reduction reaction is CO. Generally, the equilibrium potential is less negative for a proton source of lower pKa. With the water, CH_3OH or $KHCO_3$ proton source, c-CO_2RR appears consistently more thermodynamically difficult than CO_2RR (with an equilibrium potential more negative by about 0.3V), but this is not the case for the NH_4^+ proton source, where the equilibrium potential of c-CO_2RR is interestingly less negative by about 0.25V.

The influence of the proton source on the pH level is a crucial aspect to consider. Previous work on the HER showed that when the pH was increased then the equilibrium potential was shifted proportional to the change in pH according to the Nernst Equation.[41] This same trend

appeared when instead of purposely decreasing the proton concentration, a buffer at a given pH was used. Thus, to consider the effect of proton source on the PCET the pH is taken as the pK_a of the proton source. Therefore, for all calculations using methanol as the proton source the pH is taken as 15.5,[42] for H_2O as the proton source the pH is 14,[43] for $KHCO_3$ the pH is 10.3,[15] and for NH_4^+ the pH is 9.25.[44]

The equilibrium potential for the HER is independent of the solvent, but the proton source has a significant effect. This is because in the HER, the overall reaction is only dependent on the chemical potential of $H^+ + e^-$, which is related by eq 4 to the chemical potential of gas phase H_2. However, the pK_a of the proton source has a marked effect on the equilibrium potential as there are two necessary electrochemical PCET steps in the overall reaction.

The equilibrium potential of the CO_2RR is mainly affected by the proton source and, to a very small degree, by the solvent since one product is water, which is in the solvated phase with a slightly different energy in water or in methanol. Similar to the HER, the CO_2RR has 2 required electrochemical protonations. Therefore, the pK_a again has a similar effect, with less negative equilibrium potential for lower pK_a (and pH). This is seen, for example, by comparing the equilibrium potential using methanol solvent and methanol proton source with methanol solvent and NH_4^+ source for both the HER (Figure 2d) and the CO_2RR (Figure 2e). The difference in equilibrium potential is about 0.4 V for both reactions, and this trend can be seen for all other condition comparison between the HER and CO_2RR.

As shown above, if we exclude the NH_4^+ proton source, c-CO_2RR typically has the most negative equilibrium potential as compared to HER and CO_2RR. This is because of the presence of the additional chemical protonation step. This is clearly seen in equation 3, where three proton sources are involved and only two electrons. This extra chemical protonation is not present for HER and CO_2RR. c-CO_2RR has always a more negative equilibrium potential than HER across various conditions, and the difference can be significant for CH_3OH and water proton sources. Therefore, HER has a thermodynamic advantage, even if the difference is small in the case of the NH_4^+ proton source. It is thus important to find a catalyst that can offset this reaction thermodynamic constraint, and limit HER in terms of distinct overpotential and kinetic rate.

It can be seen from Figure 2 that using NH_4^+ as the proton source for the reduction of captured CO_2 provides significantly more benefit in terms of equilibrium potential than it does for HER and CO_2RR. This stems from the type of cations exchanged in the overall reaction. In the case of methanol, H_2O or $KHCO_3$ proton source an H^+ is transferred and the K^+ binds to the resulting anion. Thus, the anion (CH_3O^-, OH^-, and KCO_3^-) exchange an H^+ for a K^+. However, in the case of NH_4^+, the full proton source is NH_4ClO_4 (chosen to match experimental conditions). Therefore, during the protonation process the ClO_4^- ion exchanges a NH_4^+ with a K^+. To explore how this difference in cation affects the reactivity, the ionization potentials of the neutral species were considered. The ionization potential of H is 13.6 eV,[45] K is 4.34 eV,[46,47] and NH_4 is about 3.7 eV.[48] Thus, when the H^+ is exchanged for a K^+ in the methanol, H_2O and $KHCO_3$, this leads to a large difference in ionic interactions between the old H^+/anion pair and the new K^+/anion pair. This large difference leads to a large reaction energy for the chemical step. However, in the case of the NH_4^+ proton source, NH_4^+ and K^+ have a similar interaction with the anion, thus resulting in a

small chemical step reaction energy. Thus, the chemical step in the mechanism, and the choice of proton source, can have a large impact on the reaction energy. .

We will now consider the detailed thermodynamic reaction pathway on the Ag electrocatalyst following the mechanism of Figure 1.

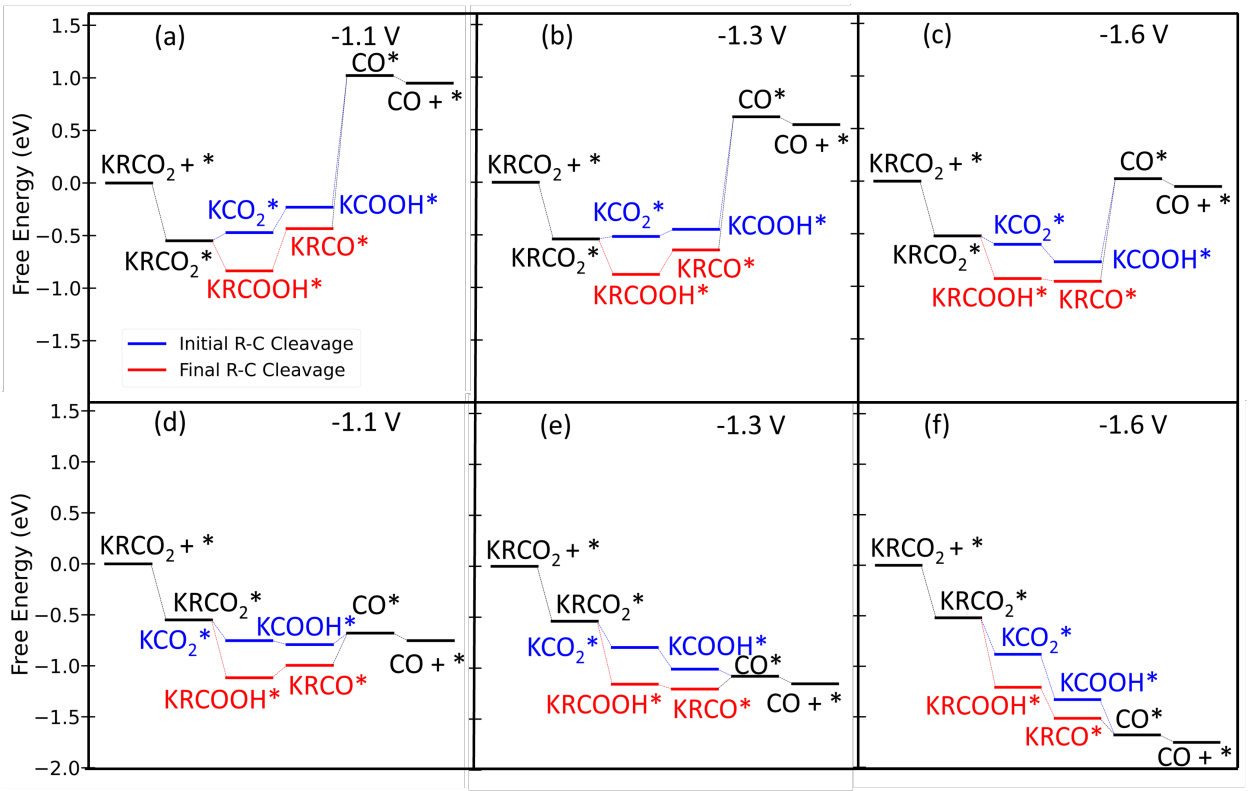

Figure 3: Thermodynamic reaction pathway for the electroreduction on Ag(111) of potassium carbamate KNH_2CO_2 in H_2O and using (a-c) water as the proton source or (d-f) NH_4^+ as the proton source as a function of potential. (a,d) -1.1 V, (b,e) -1.3 V, (c,f) -1.6 V vs. SHE. The red free energy profile corresponds to the reduction pathway highlighted in red in Figure 1 and noted "final R-C cleavage" while the blue profile depicts the pathway highlighted in blue in Figure 1 where the CO_2 complex undergoes an "initial R-C cleavage", liberating CO_2 which is further reduced to CO. The black steps involve intermediates shared by both pathways. An analogous reaction pathway on the (211) can be found in Figure S18, an example of a complete reaction pathway using all pathways from Figure 1 can be found in Figures S19-S21, and all elementary reaction energies calculated can be found in Figures S22-S26. $KRCO_2$ indicates $K^+RCO_2^-$. Short notations are used for the adsorbed species and do not imply a chemical bond between K and other atoms.

The free energy profile for the most favorable pathways for electroreduction of potassium carbamate on Ag(111) in water are shown on Figure 3 for two proton sources, water on top and NH_4^+ in the bottom and for three potential values. As mentioned previously, the reaction thermodynamics strongly depends on the proton source, the reaction being already exergonic at U=-1.1 V vs SHE for NH_4^+, and still barely exergonic at U=-1.6 V for H_2O. For the reduction

mechanism of captured CO_2, various orders can be proposed between the two PCET and the chemical protonation step. Our calculations however clearly show that only one order is favorable, where the two PCET occur first and the chemical protonation last. Indeed, earlier chemical protonation steps are markedly endergonic, while the last C-O cleavage step is the least endergonic and can more reasonably proceed in the absence of electrochemical assistance. Three paths on Figure 1 correspond to that favorable order. The common first step is the adsorption of the captured CO_2 complex $KRCO_2$ on the Ag(111) surface. This adsorption is rather strong, and its free energy is only weakly dependent on the potential, since this is not an electrochemical step. After this adsorption step several possibilities occur and the most favorable two are shown on Figure 3. The initial cleavage of the R-C bond assisted by PCET (in blue both on Figure 1 and Figure 3) produces $*CO_2$ and adsorbed K. A second PCET, markedly potential dependent, gives *COOH. At this point we have already involved two electrons along the blue paths of Figure 3, so that the final step of C-OH bond cleavage producing CO needs to be thermal, assisted by the proton donor XH. This step is strongly dependent on the nature of the proton source: at mildly negative potential (U=-1.1 V) it is markedly uphill for the water proton source, but only weakly uphill for the NH_4^+ proton source. Despite being a chemical step, it has some potential dependence, and is favored at more negative potential. It should be noted that this pathway for c-CO_2RR, initiated by de-coordination of the capture agent and production of adsorbed CO_2, is distinct from that of CO_2RR. The reactant is captured CO_2, which reacts at the electrochemical interface with 3 proton sources and two electrons. For CO_2RR, the reactant is CO_2 from the bulk of the solution (in equilibrium with captured CO_2) and two proton sources and two electrons are involved.

The other option after adsorption of $KRCO_2$ is to follow the red path where an O atom is protonated by PCET to form KRCOOH, a step which is weakly potential dependent. A PCET assisted C-O cleavage follows, this time markedly potential dependent as usual for a PCET, giving KRCO. The R-C bond cleavage then occurs as the last, chemical, step assisted by the proton donor XH to give CO. Again, this final step is strongly dependent on the proton source, difficult with H_2O and much easier with NH_4^+. One can note that the influence of the proton source is to control the thermodynamics: with water the thermodynamics is not very favorable, so that the initial steps with negative ΔG must be compensated by uphill later steps. This is not the case with NH_4^+ where the thermodynamics is much more favorable. CO desorption, easy on Ag(111), completes the catalytic cycle.

It can be underlined that some unusual potential dependence occurs, with some PCET steps being weakly potential dependent and some chemical steps being potential dependent. This comes from the fact that the K^+ cation plays different roles along the reaction pathway.

The initial captured CO_2 complex is an anion RCO_2^- and the role of K^+ is to stabilize this complex so that it can approach the electrode at negative potential, as the bare anion would suffer sever electrostatic repulsion. However, after the first PCET where the anionic RCO_2^- is converted to the neutral RCOOH surface species, K^+ mainly interacts with the surface, resulting in a higher electronic charge on this surface. and injects its charge into it. This is seen as a PZC shift to a more negative potential for the KRCOOH* intermediate. This PZC shift explains the low potential dependence of this PCET step. In contrast, the most thermodynamically favorable chemical step further on the path, from KRCO* and CO*, shows potential dependence while not being a PCET.

This is again explained by a shift of the PZC, triggered by a different role of potassium in the two intermediates.

Key structures along the pathways for c-CO2RR of Figure 3, using NH_3 as a capture agent, are represented in Figure 4. Additional structures with other capture agent are shown in the SI (Figures S29-S44).

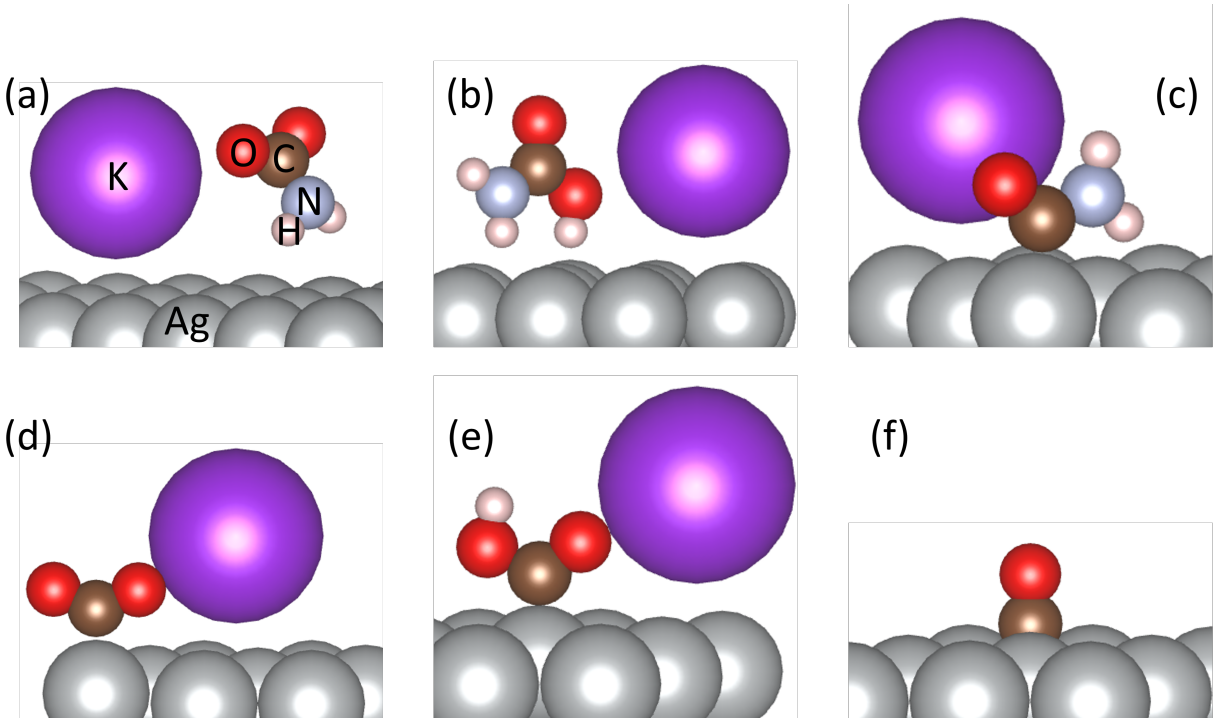

Figure 4: Structures for the major species along the pathways of Figure 3 (a) $KRCO_2$*, (b) KRCOOH*, (c) KRCO*, (d) KCO_2*, (e) KCOOH*, (f) CO*

From Figure 4, all intermediates are chemisorbed on the Ag(111) surface, with a clear chemical bond formation except for $KRCO_2$ (Figure 4a) and KRCOOH (Figure 4b) which are more weakly adsorbed (physisorbed).

Figures 3 and 4 enables us to understand in more detail the impact of the proton source on the reaction energy thermodynamics at constant potential presented above. Figure 3 clearly shows that the nature of the proton source mostly affects the required chemical protonation step, where the exchange of cation-anion pairs occurs. This is clear when comparing the reaction pathways in Figure 3 that are at the same potential but use H_2O versus NH_4^+. When H_2O is the proton source there is a significant endergonic nature of the chemical step (Figures 3a-3c, KRCO* to CO* or KCOOH* to CO*). However, this step is much easier when NH_4^+ is the proton source (Figures 3d-3f), and by -1.6 V vs. SHE (Figure 3f) the chemical step is exergonic. As explained previously, this stems from the relative instability of the proton as compared to K^+ and NH_4^+. Thus, for electroreduction of captured CO_2 to be favorable not only does the proton source's pK_a need to be low, but also the species (leading to cations) exchanged in the overall reaction need to have similar ionization potentials to decrease the reaction energy of the chemical step.

Reactivity Analysis under Different Potential

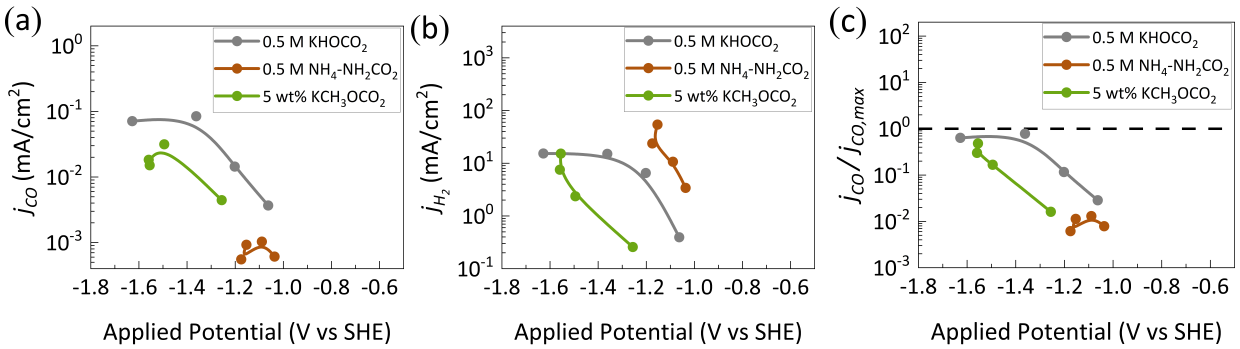

Figure 5. Partial current densities of (a) CO and (b) H_2 and (c) CO with respect to the maximum dissolved CO_2 flux as a function of applied potential. Three CO_2-captured complexes are tested: $KHOCO_2$ (Bicarbonate), NH_4-NH_2CO_2 (Ammonium Carbamate) and KCH_3OCO_2 (Methyl Carbonate).

Experimentally, the partial current densities of CO and H_2 (j_{CO} and j_{H_2}) were measured as a function of applied potential for three different capture agents to distinguish them in regard to their activity for c-CO_2RR. All the experiments reported are with freshly prepared catalyst and electrolyte as the long-time reuse of Ag films lead to different partial current densities, particularly for CO (Figure S8). $KHOCO_2$ (bicarbonate) was used directly in water while NH_4-NH_2CO_2 (Ammonium Carbamate) was used with 0.099M $KClO_4$ and 0.001M KOH to maintain the basic pH of the system and to increase the conductivity of the solution. For KCH_3OCO_2, methanol was used as the solvent, as an aqueous medium would lead to the formation of methanol and bicarbonate through the hydration of the methyl carbonate. Amine capture agents were first studied and as can be observed from Figure 5a, j_{CO} obtained for the ammonium carbamate (NH_4-NH_2CO_2) complex was the least and almost negligible compared to the methyl carbonate (KCH_3OCO_2) and bicarbonate ($KHOCO_2$) adducts although the loading of CO_2 in the solution is similar in terms of total amount of captured CO_2 in the solution. The maximum j_{CO} obtained for $KHOCO_2$ and KCH_3OCO_2 was 0.081 and 0.034 mA/cm^2 respectively. For NH_4-NH_2CO_2, HER dominated over c-CO_2RR and CO_2RR since ammonium cations present with amine-captured CO_2 can act as an efficient proton source to promote HER at the surface of the electrode.[15,16] For $KHOCO_2$, with increasing overpotentials, j_{CO} kept increasing and then reached a plateau. This also held true for j_{H_2} in $KHOCO_2$, indicating a limiting current is reached when the applied potentials are made more negative, as can be seen from Figure 5b. This initially provided evidence of dissolved CO_2 to be the main species being reduced. Small amounts of CH_4 with faradaic efficiencies of 0.04% were also observed for the two more negative potential points which were converted to equivalent amounts of CO and plotted as j_{CO} in Figure 5b for simpler interpretation. Methyl Carbonate KCH_3OCO_2 when tested for c-CO_2RR, required higher overpotentials to reach similar amounts of CO but had the least current for HER. However, it is necessary to note that j_{CO} is also a function of the unbound dissolved CO_2 in the system which is again a function of the temperature, pressure and pH of the system, that dictates the different equilibrium constants of the different equilibrium

reactions present within the system (see Figure S9). Hence, to truly capture the activity of c-CO_2RR, one must try to identify the source of carbon which could be achieved by comparing the partial current densities with the free CO_2 in the solution.

In our RCE cell, the partial pressure of CO_2 was measured from the headspace to estimate the amount of free dissolved CO_2 in the system using Henry's law. Figure 5c plots the ratio between the measured j_{CO} and the calculated maximum CO current $j_{CO,max}$ that will be obtained if the only reactant to produce CO is the unbound dissolved CO_2 in the bulk of the electrolyte. This means that at a value of 1 all the dissolved CO_2 in the bulk of the electrolyte would flow to the electrode and would be reduced to CO. For all the capture medium tested, the normalized j_{CO} reaches a value close to 1 but always stays below the limiting line, indicating that the reduced species is unbound free CO_2 present in the solution. It should be noted that the solvent used for KCH_3OCO_2 is methanol which has a higher solubility and diffusivity for CO_2 compared to water, and if these differences in intrinsic properties are not taken into consideration, it is possible to obtain erroneous normalized $j_{CO}/j_{CO,max}$ values that cross the limiting line in Figure S10. In the methanol solvent, the higher concentration of free dissolved CO_2 in the solution in equilibrium with the partial pressure of CO_2 increases the flux of CO_2 to the electrode's surface compared to the aqueous electrolytes. Also, if the CO_2-bound adduct was the active species undergoing reduction reactions, then the j_{CO} observed would be two orders of magnitude higher than what is currently obtained in our experiments. The only reacting species on silver surfaces is thus the dissolved CO_2. This dissolved CO_2 is present in very low concentration under c-CO_2RR conditions, in the order of 100 μM compared to its typical solubility of 34 mM in water at room temperature under CO_2RR conditions, which is almost three orders of magnitude lower. The low concentration of CO_2 and the unfavorable energetics for captured CO_2 to approach the surface of the catalyst could lead to proton sources to have a more favorable access to the active surface favoring HER.[15,16,49] In the capture agents tested, HER was least for the case of methyl carbonate capture complex, which is explained by the fact that the only proton source is methanol from the solvent, compared to the more Bronsted acidic and hence more efficient $KHOCO_2$ or NH_4^+ proton sources for other systems. The effect of a higher K^+ concentration was also investigated for 0.5 M NH_4-NH_2CO_2 which slightly increased the j_{CO} and suppressed j_{H_2}, but the j_{CO} still remained low to suggest that dissolved CO_2 is the reduced species (Figure S11). This indicates that alcohol-based capture agents and solvents could provide a good alternative for the electroreduction of captured CO_2, although we do not have experimental evidence of c-CO_2RR on silver.

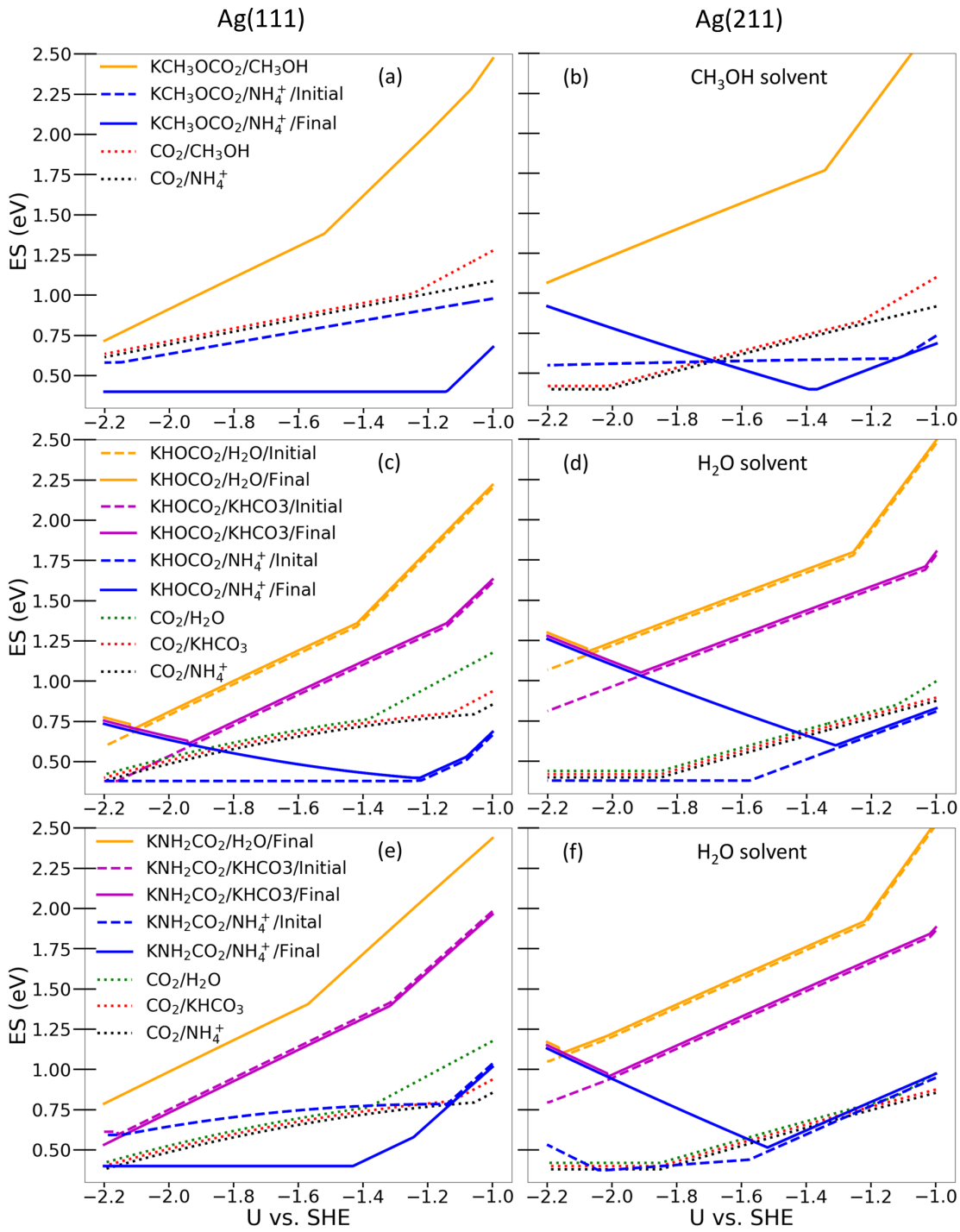

Figure 6: Calculated energetic spans (ES) for the electroreduction of captured CO_2: Three captured complexes are considered: (a,b) methyl carbonate KCH_3OCO_2, (c,d) bicarbonate $KHOCO_2$, and (e,f) carbamate KNH_2CO_2. (a,c,e) correspond to an Ag (111) catalysts surface and (b,d,f) to Ag (211) step. The reduction of non-captured CO_2 in the presence of K^+ is also considered for comparison. The legend indicates the (captured CO_2 complex $KRCO_2$) / (proton source XH)/c-CO_2RR reaction pathway. The solvent is indicated in the top right corner of each subfigure and (a,b) is methanol and in (c-f) it is H_2O. "initial" refers to the initial R-C cleavage pathway in Figure

3 and "final" refers to the final R-C cleavage pathway in Figure 3. When different pathways have the same value at a given potential the pathways have been slightly shifted to allow for all pathways to be visible. No c-CO_2RR pathway is indicated in the case where both pathways provide the same ES. The definition of the ES is detailed in SI (Figure S45).[50,51]

On the theory side, reactivity has been evaluated by using energetic span (ES) starting with the free energy pathways of Figure 3 (Figures S18-S28). In the ES model, the reactivity of a given pathway can be approximated by the largest energy difference between a transition state on the pathway in question and an intermediate on any pathway.[50,51] This way each pathway is referenced similarly to allow for a fair comparison. Transitions states/free energy barriers are required to determine the ES and explicit determination of all potential dependent free energy barriers would be a huge endeavor. All elementary reaction steps are PCET or proton transfer, and hence present strong similarity. For simplicity, we will assume that all the free energy barriers are equal, and a value of 0.4 eV has been assumed.[52–54] Our results here only focus on the influence of the different free energies for the intermediates on the reactivity and onset potential when changing capture agent and proton source, and any influence from detailed energy barriers is not taken into account. Our tests show that changing the fixed barrier value from 0.1 eV to 1.0 eV does not qualitatively change the results (Figure S46).

As explained before, to calculate the ES, the rate determining transition state does not need to be in the elementary step directly after the rate determining intermediate, and therefore it is more appropriate to use the term rate determining process rather than rate limiting step. Such a notion of rate determining process and not step is also underlying in the degree of rate control approach of microkinetics[55]. For example, in Figure 3a and b, for carbamate reduction using H_2O proton source at –1.0 and –1.3 V vs. SHE, respectively, we find that the rate determining intermediate is KRCOOH* and the rate determining TS is the one leading to the CO*intermediate. Thus, the rate determining span can be described by the KRCOOH* and CO* intermediates. However, we find that as the potential is made more negative (Figure 3c at –1.6 V vs. SHE) then the rate determining span becomes defined by KRCO* and CO*. A similar effect occurs for the NH_4^+proton source but the change in rate determining span occurs at a less negative potential than for the H_2O proton source. Therefore, we show that the rate determining process is dependent on both potential and proton source.

The resulting ES is shown in Figure 6 as a function of the potential for various combinations of capture agent, proton source and solvent. For all capture agents, the methanol or water proton source (orange lines) appear poorly reactive for electroreduction of captured CO_2. In contrast the NH_4^+ proton source (dark blue line) leads to a much better reactivity, with low ES. The "Initial R-C cleavage" and "Final R-C cleavage" pathways provide distinct ES for the NH_4^+ proton source. The most favored path is capture-agent dependent and surface dependent. For Ag(111), methanol and NH_3 capture agents favor the final cleavage of the R-C bond in the captured CO_2 complex. The H_2O capture agent and generally speaking the stepped surface Ag(211) tend to favor the initial cleavage of the capture agent.

On the lower coordination sites of (211) the adsorption of CO_2 is much more favorable than that on the (111).[56] Thus, as the potential is made more negative the adsorbed CO_2* becomes

more and more favorable as compared to the protonated complex, regardless of capture agent. When H_2O is used as the CO_2 capture agent the protonated complex is carbonic acid which is not stable because of its low pK_a.[57] Thus, it is thermodynamically more favorable for CO_2* to adsorb than the protonated complex when H_2O is the capture agent as compared to when methanol or NH_3 are used, regardless of the catalyst. Therefore, the ES for the initial R-C cleavage becomes smaller than that of the final R-C cleavage because the initial cleavage pathway is no longer hindered by the low stability of *CO_2 on the catalyst and therefore becomes more favorable than the chemical step between KRCO* and CO* required in the final cleavage pathway.

The reduction of free CO_2 is calculated to be considerably more active than that of captured CO_2 if methanol, water or bicarbonate proton sources are used, but the competition is tighter if the proton source is NH_4^+. More specifically, in that case, the reduction of captured CO_2 is more or as active as that of free CO_2. For CO_2RR, the proton source does not have a significant effect on the ES as a function of potential. This is because at even moderately negative potentials, CO_2RR ES is controlled by the adsorption of CO_2, a step not affected by the proton source. In contrast, CO_2RR is markedly affected by the choice of the Ag surface, with a better reactivity on the more open Ag(211) surface where CO_2 adsorption is stronger. Conversely, the c-CO_2RR has a larger ES on the (211) facet than the (111) terrace. Thus, c-CO_2RR is thermodynamically more favorable on atomically flat electrodes rather than on stepped surfaces.

For practical link with experiments, the ES should be associated to measurable activity descriptors, as the onset potential for the reaction. An ES of 0.75 eV corresponds at room temperature to a rate of ~1 s^{-1}. The onset potential was therefore estimated as the potential value for which the ES reaches 0.75 eV and for which the overall thermodynamics of the reaction is favorable (to make sure that the reaction is running in the right direction). The onset potential is negative in our cases. The overpotential is calculated as the absolute value of the difference between the onset potential and the equilibrium potential and is hence defined as a positive value.

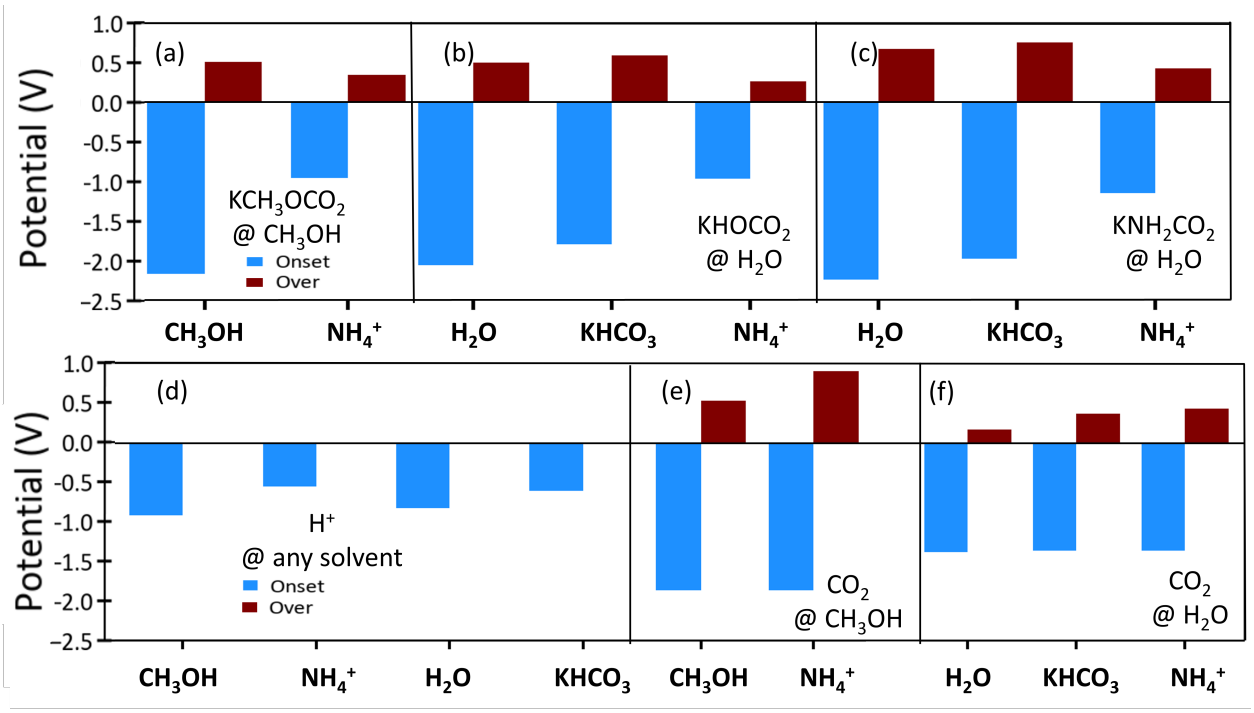

Figure 7. Calculated onset potential (blue, in Volts vs SHE) and over-potential (brown, in Volts) for the electroreduction of (a) methyl carbonate KCH_3OCO_2, (b) bicarbonate $KHOCO_2$, (c) carbamate KNH_2CO_2 on Ag (111) using the various solvent-proton source combinations tested. The compound being electrochemically reduced is labeled in the top right of each panel, together with the solvent (notation: compound@solvent). The x axis denotes the proton source. Values for (d) HER, (e) CO_2RR in CH_3OH solvent and (f) CO_2RR in H_2O solvent are also given for comparison. The onset potential is defined as the least negative potential lower than the equilibrium potential at which the ES becomes equal to 0.75 eV, while the overpotential, taken as a positive value, is equal to the absolute value of the difference between the onset potential and the equilibrium potential. The pathway that has the smallest onset potential is displayed.

Figure 7 shows the calculated onset and overpotentials for the different reactions on the Ag (111) surface. An analogous figure for the stepped (211) surface can be found in Figure S47. The reduction of the captured CO_2 complexes using water or methanol solvent and proton source onsets only at rather negative potentials (about -2 V), in line with the high ES shown in Figure 6. However, the nature of the proton source has a large impact, as already noticed, and as the pK_a of the proton source decreases the onset potential becomes less negative (about -1V for NH_4^+). The over-potential is however very similar, in the range 0.3-0.6 V, with only a small decrease when switching to the NH_4^+ proton source. This means that the main influence of the proton source lies in the thermodynamic equilibrium potential, with a marked shift to less negative equilibrium potential for NH_4^+ as seen above. For the CO_2RR, the onset potential is usually not dependent on the proton source. The CO_2RR activity is however dependent on the solvent, methanol solvent yielding more negative onset potential and larger overpotential, since the adsorption of CO_2 is destabilized in methanol. Onset potentials are generally more negative for the reduction of captured CO_2, compared to free CO_2. There are however two situations where reduction of

captured CO_2 can be competitive with that of free CO_2: the use of a low pK_a proton source as NH_4^+, which makes c-CO_2RR easier without improving much CO_2RR, and the use of a solvent with a lower dielectric constant as methanol, which penalizes CO_2RR. The larger overpotential needed to reduce dissolved CO_2 in the methanol solvent is indeed observed experimentally in Figure 5 where around 0.2V of additional potential is needed to observe the same current densities for CO as those observed in the aqueous electrolytes.

However, the big competitor (and the winner) on Ag(111) is HER since its onset potential is significantly less negative than that of the reduction of captured or free CO_2. This is despite the fact that Ag is not a good HER electrocatalyst: at the relevant pH for the various proton source, the calculated onset potential is between -0.6 and -1 V. vs. SHE. Similar to the case of captured CO_2, but in a smaller magnitude, the onset potential becomes less negative if the pKa of the proton source is decreased. This proton source dependence explains the experimental trend of the H_2 current in Figure 5b. In the methanol carbonate system, the only proton source is methanol. In the bicarbonate system there is water and bicarbonate as potential proton sources, and for the carbamate system water, bicarbonate, and NH_4^+ were present. Experimentally it was observed that the production of H_2 was larger for the carbamate system than the bicarbonate system which was larger than the methanol system at the same potential. This comes from the onset potential of the HER being the most negative for methanol proton source, moderately negative for the bicarbonate proton source and the least negative for NH_4^+. Therefore, at a given potential, the hydrogen current will be larger for NH_4^+ proton source followed by bicarbonate and methanol.

Figure 7 considers a perfect Ag(111) surface, with high coordination Ag atoms. The influence of low coordination step sites has been studied by considering the Ag(211) surface for which the calculated onset and over-potential are given in Figure S47. Ag(211) includes step atoms and short (111) terrace atoms, and the best site has been considered in each case. The main influence of step sites is to render CO_2 adsorption less exergonic, and since CO_2 adsorption is the main origin of the ES for CO_2RR, the stepped Ag(211) surface generally provides less negative onset potentials for CO_2RR. Unfortunately, the influence on the c-CO_2RR is mainly opposite: with methanol, water and bicarbonate proton sources, onset potentials are more negative or impossible on Ag(211). It should be underlined however that in the case of the efficient NH_4^+ proton source, the onset potential is basically unchanged when going from to Ag(211). Figure 6 shows that for the NH_4^+ proton source the ES for the reduction of captured CO_2 has similar magnitudes regardless of facet, but on the (111) typically the complex undergoes the final R-C cleavage pathway, while for the (211) the complex undergoes initial R-C cleavage. Therefore, step sites do not help the reduction of captured CO_2, and at best do not influence it.

The main challenge is however that the competition between the reduction of captured CO_2 and HER is very difficult to overcome since they are both accelerated by the choice of a better proton source. From the calculated data of Figures 6 and 7, the reduction of potassium carbamate would appear favorable because of the presence of the NH_4^+ proton source (the onset potential is a reasonable –1.0 V vs. SHE, Figure 7c). However, this is not the case in the experiments where the CO current is low. This is because HER dominates in these conditions.

From Figure 5c, the partial current density for the methanol carbonate never crosses the transport line, implying that reduction mainly occurs on free CO_2. In the experiment methanol was the only available proton source in the methyl carbonate reaction system. From Figure 7a the onset potential for the direct reduction of methyl carbonate using methanol as the proton source is highly negative on the (111) terrace and not achievable on the (211) facet. However, in Figure 7e and Figure S47e the onset potential for CO_2RR on both facets is less negative than that of the methyl carbonate reduction. This means that most of the partial current density of CO in the methyl carbonate system is from CO_2RR, and that most of the reaction is occurring on rough surfaces.

Similarly, in the experiment trying to directly reduce $KHOCO_2$, the proton source with the lowest pK_a was $KHCO_3$. Figure 7b and Figure S47b shows that the bicarbonate reduction achieves onset at highly negative potentials on both the (111) and (211). However, from Figure 7f and S45f the CO_2RR achieves onset in water at about –1.3 V vs. SHE on both the (111) and (211). Thus, again most of the CO produced experimentally should be from the CO_2RR. Considering the more active (211) facet, the onset potential of the CO_2RR in methanol is about 0.1 V vs. SHE more negative than CO_2RR in water, thus explaining the overpotential shift between the methanol and bicarbonate systems seen in Figure 3c.

From Figure 7, it is predicted that if NH_4^+ is used as a proton source, the onset potential for captured CO_2 reduction, using any capture agent, would be less negative than when using any other proton sources. In these conditions, the onset potential for the carbamate's direct reduction is less negative than that of the CO_2RR on the (111) and similar on the (211). Thus, calculations suggest that some of the captured CO_2 complex could be reduced in these conditions.

However, it is to be noted that on the (211), onset is difficult or even impossible for proton sources with larger pK_a. This arises from the adsorption of the complex becoming less stable as the potential is increased, with eventually this adsorption becoming endergonic. Thus, what occurs is that between consecutive cycles the system gets stuck trying to adsorb more complex. When NH_4^+ proton source is used the reactivity is large enough to achieve onset at less negative potentials, where the complex adsorption is still exergonic. However, as Figure 6f shows both c-CO_2RR pathways see an increase in their energetic spans as the potential is made more negative. Thus, for proton sources with larger pK_a it is possible that onset is not achieved before the complex adsorption barrier dominates the system.

Although not experimentally tested, calculations predict that the same trend would occur if NH_4^+ proton source was used for methyl carbonate electroreduction. Thus, theoretically, methyl carbonate and carbamate have been validated to being able to be directly reduced, only considering the competition with free CO_2. However, unfortunately on Ag when NH_4^+ is used as the proton source the HER fully dominates. Therefore, methanol and amines appear to be a valid choice of capture agent for direct reduction, but this requires 1) to use a proton source with low pK_a and 2) to use a catalyst that would suppress the HER in a more drastic manner than Ag can do.

Finally, we have studied experimentally the influence of the roughness of the Ag electrode. The results obtained from the as-sputtered Ag electrodes were compared to electrochemically roughened Ag electrodes (Figure S12). It was observed experimentally that the morphology of the catalyst does indeed play a role in altering the faradaic efficiency of CO (Figure S13). For all three

capture agents, the faradaic efficiency of CO increased with more porosity, with $KHOCO_2$ and KCH_2OCO_2 producing CO with an FE of ~1% and ~1.6% respectively. It could be hypothesized that with a more porous electrode, the local pH within the pores becomes much higher than at the entrance of the pore, and that this could lead to the favorable release of CO_2 locally within the pores where it can be reduced to CO (Figure S14). However, irrespective of whether the CO_2 is released locally at the electrode surface or whether it is present in the bulk of the solution, it is still concluded that it is the reduction of CO_2 that takes place under our conditions and not the direct reduction of the CO_2-bound adduct.[32]

Conclusions

We have revealed the mechanism of the electroreduction of captured CO_2 and the influence of capture agent, proton source and solvent from a combination of theory and experiment. We show that the proton source plays a key role in the interplay of the chemistry for the electroreduction of protons, free CO_2, and captured CO_2. The direct reduction of captured CO_2 appears generally more difficult than that of free CO_2 or hydrogen, mainly on a thermodynamic aspect and for its onset potential on the Ag catalysts. However, calculations show that when using proton sources with low pKa as NH_4^+, reduction of captured CO_2 can be made markedly easier. This influence of the proton source is stronger for c-CO_2RR than for CO_2RR and HER, because reduction of captured CO_2 requires an additional chemical protonation step, compared to HER or CO_2RR. With NH_4^+ as a proton source, and NH_3 as capture agents, the reduction of captured CO_2 can be theoretically made easier than that of free CO_2. However, HER is also facilitated by a good proton source, so that electroreduction of captured CO_2 cannot compete with HER on Ag, despite Ag being a poor HER catalyst. In our experiment, the CO product is seen from the electroreduction of dissolved CO_2 and not of captured CO_2. Alcohol-based capture agents enable to decrease the HER current but required higher overpotentials to reach similar amounts of CO than the other two tested capture agents.

On the mechanistic aspect of c-CO_2RR, the first two steps are PCET, while the third and last step of C-O bond cleavage producing CO is a chemical protonation. Indeed, the last C-O cleavage step is the least endergonic and can more reasonably proceed in the absence of electrochemical assistance. The influence of the proton source is mainly operating on this required chemical protonation step, where an exchange of cation-anion pairs occurs. As a result, the methanol or water proton source appear poorly reactive for electroreduction of captured CO_2 and electroreduction onsets only at negative potentials. In contrast the NH_4^+ proton source leads to a much better reactivity, with a markedly less negative onset. The most favored path for c-CO_2RR, in terms or order of steps, is capture-agent dependent and surface dependent, and steps do not appear as favorable for this reaction.

The reduction of captured CO_2 generally requires more negative onset potentials when compared to free CO_2, except when using a low pK_a proton source as NH_4^+. However, HER onset at less negative potential than CO_2RR or c-CO_2RR on Ag, for all the capture agent / proton source / solvent combination that we have considered, rendering the selectivity of the c-CO_2RR highly challenging on Ag.

Therefore, the electroreduction of captured CO_2 appears as a difficult reaction on Ag catalysts, because the reaction is thermodynamically challenging and requires onset potentials that are more negative than that of CO_2RR and even more than that of HER. c-CO_2RR requires an efficient proton source, but this does not improve the completion with HER since HER is also accelerated. The only way forward to see efficient captured CO_2 reduction from this study appears to be the combination of a good proton source, with a catalyst that severely hinders HER.

Supplementary Information

Additional experimental and computational methods are discussed in the attached supplementary information. The experimental portion contains additional characterization, schematics, and experimental results. The computational section shows all structures and computational parameters used, as well as additional reaction pathways and elementary reaction data.

Acknowledgments

We would like to acknowledge and thank the University of California Office of the President and the National Laboratory Research Fees Program for their support of our ongoing work in this area with award L22CR4468, which supports the Center for Direct Conversion of Captured CO_2 into Chemicals and Fuels. Computational calculations were run on the UCLA Institute for Digital Research and Education's Research Technology Group's cluster Hoffman2 and Advanced Cyberinfrastructure Coordination Ecosystem: Services & Support's (ACCESS) clusters Expanse and Bridges2 through the allocation CHE170060 at the San Diego Supercomputing Center through ACCESS. We would also like to thank the California NanoSystems Institute for the generous access to their facilities for using the sputtering machine to prepare the Ag catalysts. We would also like to acknowledge and thank Dr. Kangze Shen for his work on the pK_a/pH effects on the equilibrium potential of the HER. We would also like to acknowledge and thank Jounghwan Choi for his help with running XPS. The computational data in this paper has been adapted from the Master of Science Thesis of Robert Michael Kowalski, entitled: "Comparing the reactivity of capture agents and proton source for captured carbon dioxide reduction reaction. A theoretical assessment." (University of California, Los Angeles).

References

1. Cheng, W.; Dan, L.; Deng, X.; Feng, J.; Wang, Y.; Peng, J.; Tian, J.; Qi, W.; Liu, Z.; Zheng, X.; Zhou, D.; Jiang, S.; Zhao, H.; Wang, X. Global Monthly Gridded Atmospheric Carbon Dioxide Concentrations under the Historical and Future Scenarios. *Sci Data* **2022**, *9* (1). https://doi.org/10.1038/s41597-022-01196-7.

(2) Al-Mamoori, A.; Krishnamurthy, A.; Rownaghi, A. A.; Rezaei, F. Carbon Capture and Utilization Update. *Energy Technology* **2017**, *5* (6), 834–849. https://doi.org/10.1002/ente.201600747.

(3) Cheng, D.; Wei, Z.; Zhang, Z.; Broekmann, P.; Alexandrova, A. N.; Sautet, P. Restructuring and Activation of Cu(111) under Electrocatalytic Reduction Conditions. *Angewandte Chemie - International Edition* **2023**, *62* (20). https://doi.org/10.1002/anie.202218575.

(4) Cheng, D.; Zhang, G.; Li, L.; Shi, X.; Zhen, S.; Zhao, Z. J.; Gong, J. Guiding Catalytic CO_2 Reduction to Ethanol with Copper Grain Boundaries. *Chem Sci* **2023**, *14* (29), 7966–7972. https://doi.org/10.1039/d3sc02647g.

(5) Nitopi, S.; Bertheussen, E.; Scott, S. B.; Liu, X.; Engstfeld, A. K.; Horch, S.; Seger, B.; Stephens, I. E. L.; Chan, K.; Hahn, C.; Nørskov, J. K.; Jaramillo, T. F.; Chorkendorff, I. Progress and Perspectives of Electrochemical CO_2 Reduction on Copper in Aqueous Electrolyte. *Chemical Reviews* **2019**, *119* (12), 7610–7672. https://doi.org/10.1021/acs.chemrev.8b00705.

(6) Kuhl, K. P.; Hatsukade, T.; Cave, E. R.; Abram, D. N.; Kibsgaard, J.; Jaramillo, T. F. Electrocatalytic Conversion of Carbon Dioxide to Methane and Methanol on Transition Metal Surfaces. *J Am Chem Soc* **2014**, *136* (40), 14107–14113. https://doi.org/10.1021/ja505791r.

(7) Kumari, S.; Alexandrova, A. N.; Sautet, P. Nature of Zirconia on a Copper Inverse Catalyst Under CO_2 Hydrogenation Conditions. *J Am Chem Soc* **2023**, *145* (48), 26350–26362. https://doi.org/10.1021/jacs.3c09947.

(8) Siegel, R. E.; Pattanayak, S.; Berben, L. A. Reactive Capture of CO_2: Opportunities and Challenges. *ACS Catal* **2023**, *13* (1), 766–784. https://doi.org/10.1021/acscatal.2c05019.

(9) Hack, J.; Maeda, N.; Meier, D. M. Review on CO_2 Capture Using Amine-Functionalized Materials. *ACS Omega* **2022**, *7* (44), 39520–39530. https://doi.org/10.1021/acsomega.2c03385.

(10) Dziejarski, B.; Serafin, J.; Andersson, K.; Krzyżyńska, R. CO_2 Capture Materials: A Review of Current Trends and Future Challenges. *Materials Today Sustainability* **2023**, *24*, 100483 https://doi.org/10.1016/j.mtsust.2023.100483.

(11) Davran-Candan, T. DFT Modeling of CO_2 Interaction with Various Aqueous Amine Structures. *Journal of Physical Chemistry A* **2014**, *118* (25), 4582–4590. https://doi.org/10.1021/jp503929g.

(12) Zhang, Z.; Kummeth, A. L.; Yang, J. Y.; Alexandrova, A. N. Inverse Molecular Design of Alkoxides and Phenoxides for Aqueous Direct Air Capture of CO_2 *Proc Natl Acad Sci*, **2022**, *119* (25), https://doi.org/10.1073/pnas.2123496119.

(13) Appel, A. M.; Yang, J. Y. Maximum and Comparative Efficiency Calculations for Integrated Capture and Electrochemical Conversion of CO_2. *ACS Energy Letters* **2024**, *9* (2), 768–770. https://doi.org/10.1021/acsenergylett.3c02489.

(14) Orestes, E.; Machado Ronconi, C.; Carneiro, J. W. de M. Insights into the Interactions of CO2 with Amines: A DFT Benchmark Study. *Physical Chemistry Chemical Physics* **2014**, *16* (32), 17213–17219. https://doi.org/10.1039/c4cp02254h.

(15) Leverick, G.; Bernhardt, E. M.; Ismail, A. I.; Law, J. H.; Arifutzzaman, A.; Aroua, M. K.; Gallant, B. M. Uncovering the Active Species in Amine-Mediated CO_2 Reduction to CO on Ag. *ACS Catal* **2023**, *13* (18), 12322–12337. https://doi.org/10.1021/acscatal.3c02500.

(16) Safipour, J.; Weber, A. Z.; Bell, A. T. Detrimental Effects of Monoethanolamine and Other Amine-Based Capture Agents on the Electrochemical Reduction of CO_2. *ACS Energy Lett* **2023**, *8* (12), 5012–5017. https://doi.org/10.1021/acsenergylett.3c01953.

(17) Shen, K.; Cheng, D.; Reyes-Lopez, E.; Jang, J.; Sautet, P.; Morales-Guio, C. G. On the Origin of Carbon Sources in the Electrochemical Upgrade of CO_2 from Carbon Capture Solutions. *Joule* **2023**, *7* (6), 1260–1276. https://doi.org/10.1016/j.joule.2023.05.010.

(18) Schüler, N.; Hecht, K.; Kraut, M.; Dittmeyer, R. On the Solubility of Carbon Dioxide in Binary Water-Methanol Mixtures. *J Chem Eng Data* **2012**, *57* (8), 2304–2308. https://doi.org/10.1021/je300332b.

(19) Bao, F.; Kemppainen, E.; Dorbandt, I.; Bors, R.; Xi, F.; Schlatmann, R.; van de Krol, R.; Calnan, S. Understanding the Hydrogen Evolution Reaction Kinetics of Electrodeposited Nickel-Molybdenum in Acidic, Near-Neutral, and Alkaline Conditions. *ChemElectroChem* **2021**, *8* (1), 195–208. https://doi.org/10.1002/celc.202001436.

(20) Bashiri, A.; Sufali, A.; Golmohammadi, M.; Mohammadi, A.; Maleki, R.; Jamal Sisi, A.; Khataee, A.; Asadnia, M.; Razmjou, A. Unveiling the Mechanisms of Catalytic CO_2 Electroreduction through Machine Learning. *Ind Eng Chem Res* **2023**. https://doi.org/10.1021/acs.iecr.3c02698.

(21) Laursen, A. B.; Varela, A. S.; Dionigi, F.; Fanchiu, H.; Miller, C.; Trinhammer, O. L.; Rossmeisl, J.; Dahl, S. Electrochemical Hydrogen Evolution: Sabatier's Principle and the Volcano Plot. *J Chem Educ* **2012**, *89* (12), 1595–1599. https://doi.org/10.1021/ed200818t.

(22) Quaino, P.; Juarez, F.; Santos, E.; Schmickler, W. Volcano Plots in Hydrogen Electrocatalysis-Uses and Abuses. *Beilstein Journal of Nanotechnology* **2014**, *5* (1), 846–854. https://doi.org/10.3762/bjnano.5.96.

(23) Kresse, G.; Furthmüller, J. Efficiency of Ab-Initio Total Energy Calculations for Metals and Semiconductors Using a Plane-Wave Basis Set. *Comp. Mater. Sci.* **1996**, *6* (1). https://doi.org/10.1016/0927-0256(96)00008-0.

(24) Kresse, G.; Furthmüller, J. Efficient Iterative Schemes for Ab Initio Total-Energy Calculations Using a Plane-Wave Basis Set. *Phys. Rev. B.* **1996**, *54* (16). https://doi.org/10.1103/PhysRevB.54.11169.

(25) Grimme, S.; Antony, J.; Ehrlich, S.; Krieg, H. A Consistent and Accurate Ab Initio Parametrization of Density Functional Dispersion Correction (DFT-D) for the 94 Elements H-Pu. *Journal of Chemical Physics* **2010**, *132* (15). https://doi.org/10.1063/1.3382344.

(26) Mathew, K.; Sundararaman, R.; Letchworth-Weaver, K.; Arias, T. A.; Hennig, R. G. Implicit Solvation Model for Density-Functional Study of Nanocrystal Surfaces and Reaction Pathways. *Journal of Chemical Physics* **2014**, *140* (8). https://doi.org/10.1063/1.4865107.

(27) Mathew, K.; Kolluru, V. S. C.; Mula, S.; Steinmann, S. N.; Hennig, R. G. Implicit Self-Consistent Electrolyte Model in Plane-Wave Density-Functional Theory. *Journal of Chemical Physics* **2019**, *151* (23). https://doi.org/10.1063/1.5132354.

(28) Steinmann, S. N.; Michel, C.; Schwiedernoch, R.; Filhol, J. S.; Sautet, P. Modeling the HCOOH/CO_2 Electrocatalytic Reaction: When Details Are Key. *ChemPhysChem* **2015**, *16* (11), 2307–2311. https://doi.org/10.1002/cphc.201500187.

(29) Steinmann, S. N.; Sautet, P. Assessing a First-Principles Model of an Electrochemical Interface by Comparison with Experiment. *Journal of Physical Chemistry C* **2016**, *120* (10), 5619–5623. https://doi.org/10.1021/acs.jpcc.6b01938.

(30) Steinmann, S. N.; Michel, C.; Schwiedernoch, R.; Sautet, P. Impacts of Electrode Potentials and Solvents on the Electroreduction of CO_2: A Comparison of Theoretical Approaches. *Physical Chemistry Chemical Physics* **2015**, *17* (21), 13949–13963. https://doi.org/10.1039/c5cp00946d.

(31) Hupp, J. T.; Larkin, D.; Weaver, M. J. Specific adsorption of halide and pseudohalide ions at electrochemically roughened versus smooth silver-aqueous interfaces. *Surface Science*. **1983**, *125* (2), 429-451. https://doi.org/10.1016/0039-6028(83)90576-9

(32) Jang, J.; Rüscher, M.; Winzely, M.; Morales-Guio, C. G. Gastight Rotating Cylinder Electrode: Toward Decoupling Mass Transport and Intrinsic Kinetics in Electrocatalysis. *AIChE Journal* **2022**, *68* (5). https://doi.org/10.1002/aic.17605.

(33) Décultot, M.; Ledoux, A.; Fournier-Salaün, M. C.; Estel, L. Solubility of CO_2 in Methanol, Ethanol, 1,2-Propanediol and Glycerol from 283.15 K to 373.15 K and up to 6.0 MPa. *Journal of Chemical Thermodynamics* **2019**, *138*, 67–77. https://doi.org/10.1016/j.jct.2019.05.003.

(34) Chiehming J, C.; Kou-Lung, C.; Chang-Yih, D. A New Apparatus for the Determination of P-x-y Diagrams and Henry's Constants in High Pressure Alcohols with Critical Carbon Dioxide. *The Journal of Supercritical Fluids*. **1998,** *12* (3), 223-237. https://doi.org/10.1016/S0896-8446(98)00076-X

(35) Frank, M. J. W.; Kuipers, J. A. M.; Van Swaaij, W. P. M. Diffusion Coefficients and Viscosities of CO_2 + H_2O, CO_2 + CH_3OH, NH_3 + H_2O, and NH_3 + CH_3OH Liquid Mixtures. *J. Chem Eng. Data.* **1996**, *41* (2), 297-302. https://doi.org/10.1021/je950157k

(36) Pan, B.; Wang, Y.; Li, Y. Understanding and leveraging the Effect of Cations in the Electrical Double Layer for Electrochemical CO_2 Reduction. *Chem Catalysis*. **2022**, *2*, 1267–1276. https://doi.org/10.1016/j.checat.2022.03.012.

(37) Lee, G.; Li, Y. C.; Kim, J. Y.; Peng, T.; Nam, D. H.; Rasouli, A. S.; Li, F.; Luo, M.; Ip, A. H.; Joo, Y. C.; Sargent, E. H. Electrochemical Upgrade of CO_2 from Amine Capture Solution. *Nat Energy* **2021**, *6* (1), 46–53. https://doi.org/10.1038/s41560-020-00735-z.

(38) Marcandalli, G.; Monteiro, M. C. O.; Goyal, A.; Koper, M. T. M. Electrolyte Effects on CO_2 Electrochemical Reduction to CO. *Acc Chem Res* **2022**, *55* (14), 1900–1911. https://doi.org/10.1021/acs.accounts.2c00080.

(39) Zhang, Z.; Li, H.; Shao, Y.; Gan, L.; Kang, F.; Duan, W.; Hansen, H. A.; Li, J. Molecular Understanding of the Critical Role of Alkali Metal Cations in Initiating CO_2 Electroreduction on Cu(100) Surface. *Nat Commun* **2024**, *15* (1). https://doi.org/10.1038/s41467-024-44896-x.

(40) Nørskov, J. K.; Rossmeisl, J.; Logadottir, A.; Lindqvist, L.; Kitchin, J. R.; Bligaard, T.; Jónsson, H. Origin of the Overpotential for Oxygen Reduction at a Fuel-Cell Cathode. *Journal of Physical Chemistry B* **2004**, *108* (46), 17886–17892. https://doi.org/10.1021/jp047349j.

(41) Lamoureux, P. S.; Singh, A. R.; Chan, K. PH Effects on Hydrogen Evolution and Oxidation over Pt(111): Insights from First-Principles. *ACS Catal* **2019**, *9* (7), 6194–6201. https://doi.org/10.1021/acscatal.9b00268.

(42) Ballinger, P; Long, F. A. Acid Ionization Constants of Alcohols. II. Acidities of Some Substituted Methanols and Related Compounds. *J. Am. Chem. Soc.*, **1960**, *82* (4), 795–798.

(43) Silverstein, T. P.; Heller, S. T. pKa Values in the Undergraduate Curriculum: What Is the Real pKa of Water? *J Chem Educ* **2017**, *94* (6), 690–695. https://doi.org/10.1021/acs.jchemed.6b00623.

(44) Khoo, K. H.; Culberson, C. H.; Bates, R. G. Thermodynamics of the Dissociation of Ammonium Ion in Seawater from 5 to 40^{O}C. *Journal of Solution Chemistry*, **1977**, *6*, 281–290. https://doi.org/10.1007/BF00645459.

(45) Garcia, J. D.; Mace, J. E. Energy Level and Line Tables for One-Electron Atomic Spectra. *J. Opt. Soc. Am.*, **1965**, *55* (6), 654–685. https://doi.org/10.1364/JOSA.55.000654.

(46) Foster, P. J.; Leckenby, R. E.; Robbins, E. J. The ionization potentials of clustered alkali metal atoms. *J. Phys. B: Atomic and Molecular Physics*, **1969**, *2*, 478, https://doi.org/10.1088/0022-3700/2/4/307.

(47) Herrmann, A.; Schumacher, E.; Wöste, L. Preparation and Photoionization Potentials of Molecules of Sodium, Potassium, and Mixed Atoms. *J Chem Phys* **1978**, *68* (5), 2327–2336. https://doi.org/10.1063/1.436003.

(48) Wight, G.-R.; Brion, C. E. Estimation of the excitation and ionization energies of NH_4, H_3O and H_2F radicals using core analogies applied to K-shell electron energy loss spectra. *Chem. Phys. Letters* **1974,** *26* (4), 607–609. https://doi.org/10.1016/0009-2614(74)80427-6

(49) Choi, J.; Chiu, S.; Banerjee, A.; Sacci, R. L.; Veith, G. M.; Stieber, C.; Hahn, C.; Alexandrova, A. N.; Morales-Guio, C. G. Direct Electrochemical Reduction of Ammonium Carbamate on Transition Metal Surfaces: Finding Activity and Stability Descriptors beyond Those for CO_2 Reduction. *ChemRxiv* **2024**, https://doi.org/10.26434/chemrxiv-2024-5xsp5. This content is a preprint and has not been peer-reviewed.

(50) Kozuch, S.; Shaik, S. A Combined Kinetic-Quantum Mechanical Model for Assessment of Catalytic Cycles: Application to Cross-Coupling and Heck Reactions. *J Am Chem Soc* **2006**, *128* (10), 3355–3365. https://doi.org/10.1021/ja0559146.

(51) Kozuch, S.; Shaik, S. How to Conceptualize Catalytic Cycles? The Energetic Span Model. *Acc Chem Res* **2011**, *44* (2), 101–110. https://doi.org/10.1021/ar1000956.

(52) Shi, C.; Chan, K.; Yoo, J. S.; Nørskov, J. K. Barriers of Electrochemical CO2 Reduction on Transition Metals. *Org Process Res Dev* **2016**, *20* (8), 1424–1430. https://doi.org/10.1021/acs.oprd.6b00103.

(53) Liu, X.; Xiao, J.; Peng, H.; Hong, X.; Chan, K.; Nørskov, J. K. Understanding Trends in Electrochemical Carbon Dioxide Reduction Rates. *Nat Commun* **2017**, *8*. https://doi.org/10.1038/ncomms15438.

(54) Chen, L. D.; Urushihara, M.; Chan, K.; Nørskov, J. K. Electric Field Effects in Electrochemical CO_2 Reduction. *ACS Catal* **2016**, *6* (10), 7133–7139. https://doi.org/10.1021/acscatal.6b02299.

(55) Campbell, C. T. The Degree of Rate Control: A Powerful Tool for Catalysis Research. ACS *Catal*. **2017**, *7* (4), 2770-2779. https://doi.org/10.1021/acscatal.7b00115.

(56) Jin, W.; Wang, Y.; Liu, T.; Ding, C.; Guo, H. CO_2 Chemisorption and Dissociation on Flat and Stepped Transition Metal Surfaces. *Appl Surf Sci* **2022**, *599*. https://doi.org/10.1016/j.apsusc.2022.154024.

(57) Pines, D.; Ditkovich, J.; Mukra, T.; Miller, Y.; Kiefer, P. M.; Daschakraborty, S.; Hynes, J. T.; Pines, E. How Acidic Is Carbonic Acid? *Journal of Physical Chemistry B* **2016**, *120* (9), 2440–2451. https://doi.org/10.1021/acs.jpcb.5b12428.

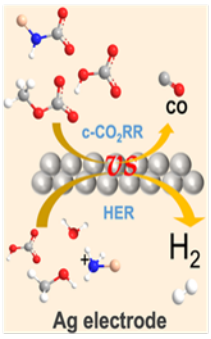
CO
c-CO2RR
OS
HER
H2
Ag electrode

Facet & Roughness
Capture Agent
Proton Source

TOC Graphic